Supporting Information for

Correlating Light Absorption with Various Nanostructure Geometries in Vertically Aligned Si Nanowire Arrays

Yi-Seul Park and Jin Seok Lee[*]

Department of Chemistry, Sookmyung Women's University, Seoul 04310, Korea

[*]E-mail: jinslee@sookmyung.ac.kr

This PDF file includes:

Section S1. KrF stepper lithography.

The patterned *v*-SiNW arrays were synthesized from AuND patterns fabricated by KrF stepper lithography as described in Figure 1, which shows the scheme of KrF stepper lithography for AuND patterning. First, the KrF laser was passed through the mask forming an image of the mask pattern. The image was focused and reduced by a lens and projected onto the surface of a Si(111) wafer coated with a photosensitive material (PR). The size of the pattern image in the mask was reduced by 4-fold compared to the original pattern area. When the wafer was processed in the stepper, the pattern on the mask, which may contain a number of individual patterns, was exposed repeatedly across the surface of the wafer in a grid. The KrF stepper lithography receives its name because it moves or steps the wafer from one location to another. This is accomplished by moving the wafer back and forth in two dimensions under the lens of the stepper.

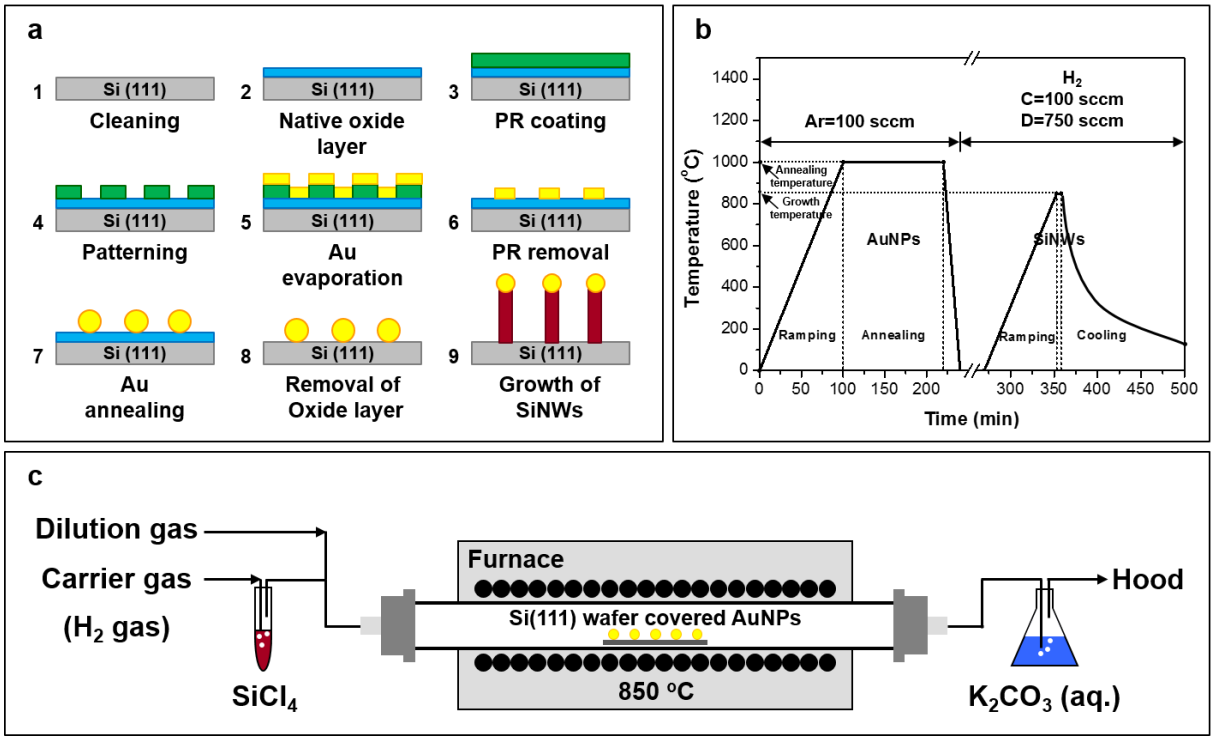

Figure S1. Experimental details. (a) Illustration of the growth process used for obtaining *v*-SiNW arrays with AuNDs, patterned on a Si (111) substrate, as the catalyst. (1) Cleaning of the Si(111) wafer, (2) formation of a native oxide layer on the substrate by thermal annealing, (3) PR coating, (4) PR patterning using KrF stepper lithography, (5) Au deposition by e-beam evaporation, (6) removal of PR, (7) Au annealing, (8) removal of the oxide layer, and (9) SiNW growth. (b) Reaction diagram consisting of the two steps including the formation of the AuNPs and growth of SiNWs. (C = carrier gas, D = diluent gas) (c) Schematic of the furnace used for the synthesis of SiNWs.

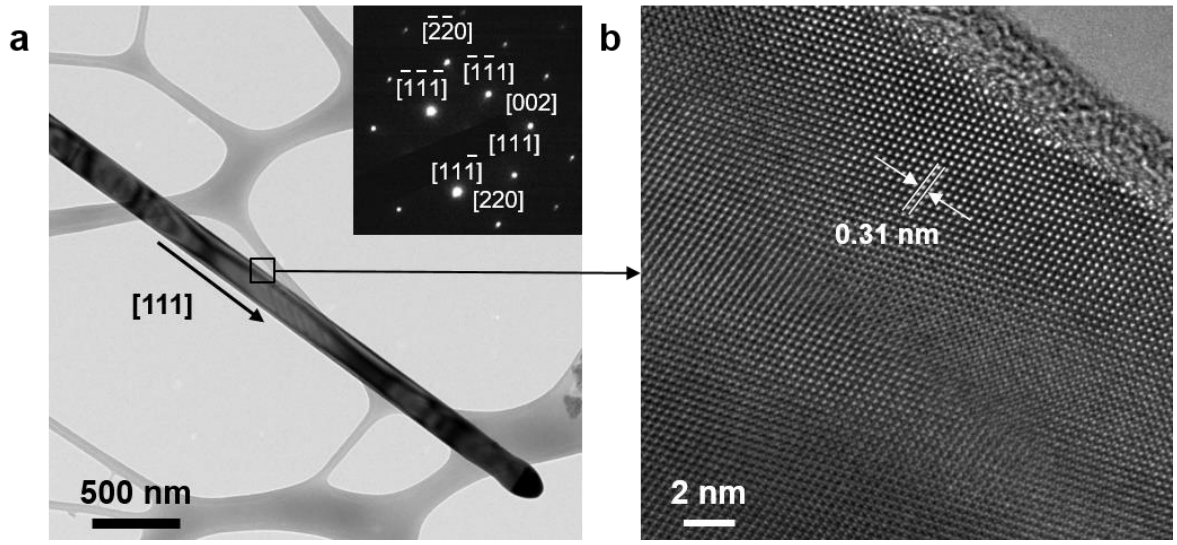

Figure S2. Characterization of a SiNW. (a) Low-magnification TEM image of a SiNW. Inset of (a) shows the selected area electron diffraction (SAED) pattern indexed for crystalline cubic Si. (b) High-resolution TEM (HRTEM) image acquired from the area designated in (a).

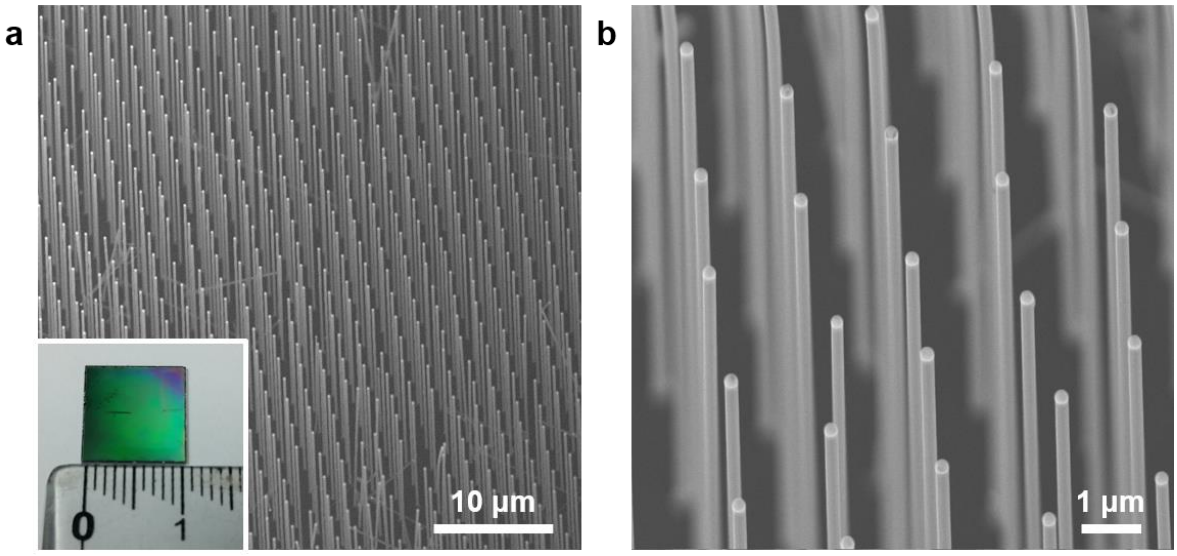

Figure S3. Synthesis of *v*-SiNW arrays in a large area. Tilt-view (20°) (a) low-magnification and (b) high-magnification SEM images of *v*-SiNWs after VLS growth with diameter D = 200 nm, pitch P = 2 μm, and length L = 25 μm. The inset of (a) shows the photograph with *v*-SiNW arrays of an area of 1cm^2.

Section S2. Strategy of AuND diameter control

The diameter of the *v*-SiNWs can be controlled through the height of the AuNDs with a consistent diameter. Figure S4 shows the overall strategy and results of diameter control in AuNPs and SiNWs. First, the SEM images of AuNPs annealed from hexagonally arrayed AuNDs patterns with heights of 30, 110, and 260 nm are shown in Figure S4a–c**,** respectively. It is possible to predict the diameter of the AuNPs using the volume relationship between AuNDs and AuNPs as spherical AuNPs are formed by annealing AuNDs. Hence, we can consider that the volume of the AuNDs is equal to that of the AuNP, which is illustrated in the inset of Figure S4d. The diameter of the SiNWs was determined by the diameter of the AuNPs because the SiNWs were synthesized by supersaturation of the Si precursor at the interface between the AuNPs and the substrate. Therefore, the diameter of the AuNPs was determined by the desired diameter of the SiNWs. The volume of AuNDs and AuNPs were represented by Equations (1) and (2).

(1) Volume of AuND: $V_{AuND}=\pi r_{AuND}^2 h$

(2) Volume of AuNP: $V_{AuNP}=3/4(\pi r_{AuNP})^3$

In the above equations, r_{AuND} and r_{AuNP} are the radii of the AuND and AuNP, respectively, and h is the height of the AuND. The radius of the AuND is fixed at 200 nm and the radius of the AuNP is decided in accordance with the desired radius of the SiNW. To vary the diameter of the AuNP, which affects the diameter of the SiNW, the volume of the AuNP needs to be controlled assuming that the volume of AuND and AuNP are the same. This can be used to regulate the volume of AuND by controlling the height of AuND because it correlates with the volume of the AuNP. As a result, AuNPs with diameters of 204 ± 15.42, 280 ± 18.86, and 413 ± 11.37 nm were

obtained by annealing from AuNDs with heights of 30, 110, and 260 nm, respectively. Figure S4d shows the calculated and experimental values of the diameters of AuNPs. The experimental values of AuNPs corresponded well with the calculated values.

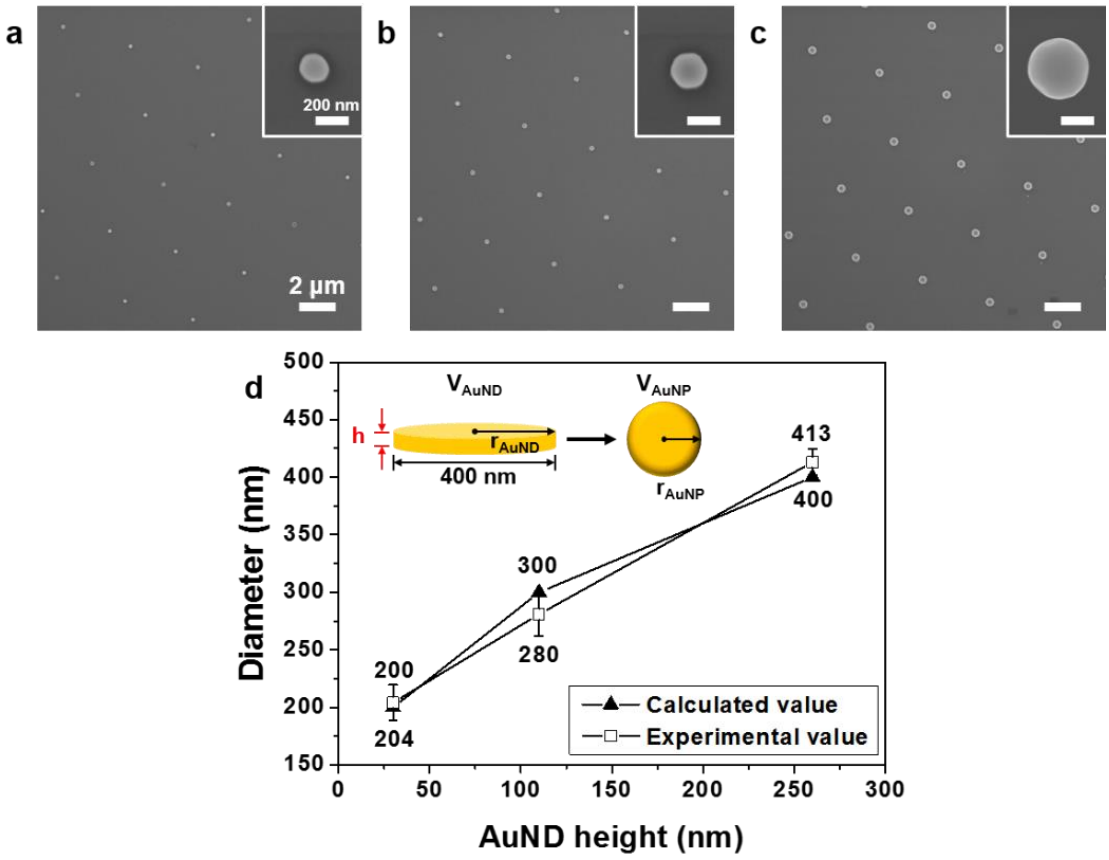

Figure S4. Correlation between the AuND height and AuNP diameter. SEM images of AuNPs with diameters of (a) 200, (b) 300, and (c) 400 nm for fixed pitch (P = 4 μm), annealed at 1000 °C for 2 h. (d) AuNP diameter as a function of the height of the AuND pattern for the calculated and experimental values. Inset of (d) shows the relationship between AuND height and AuNP diameter.

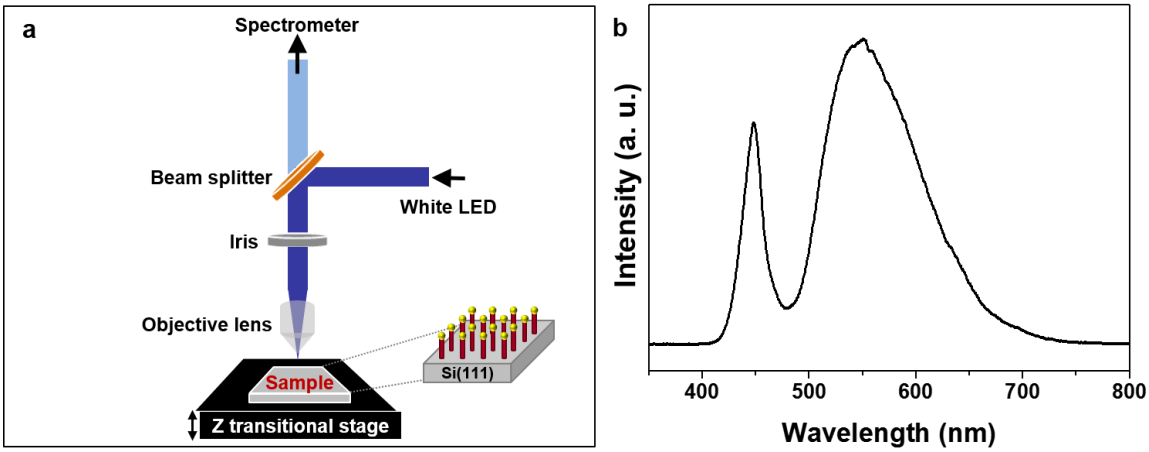

Figure S5. Optical measurement setup. (a) Schematic diagrams of the experimental set up. (b) The spectral output of the white LED used in this study.

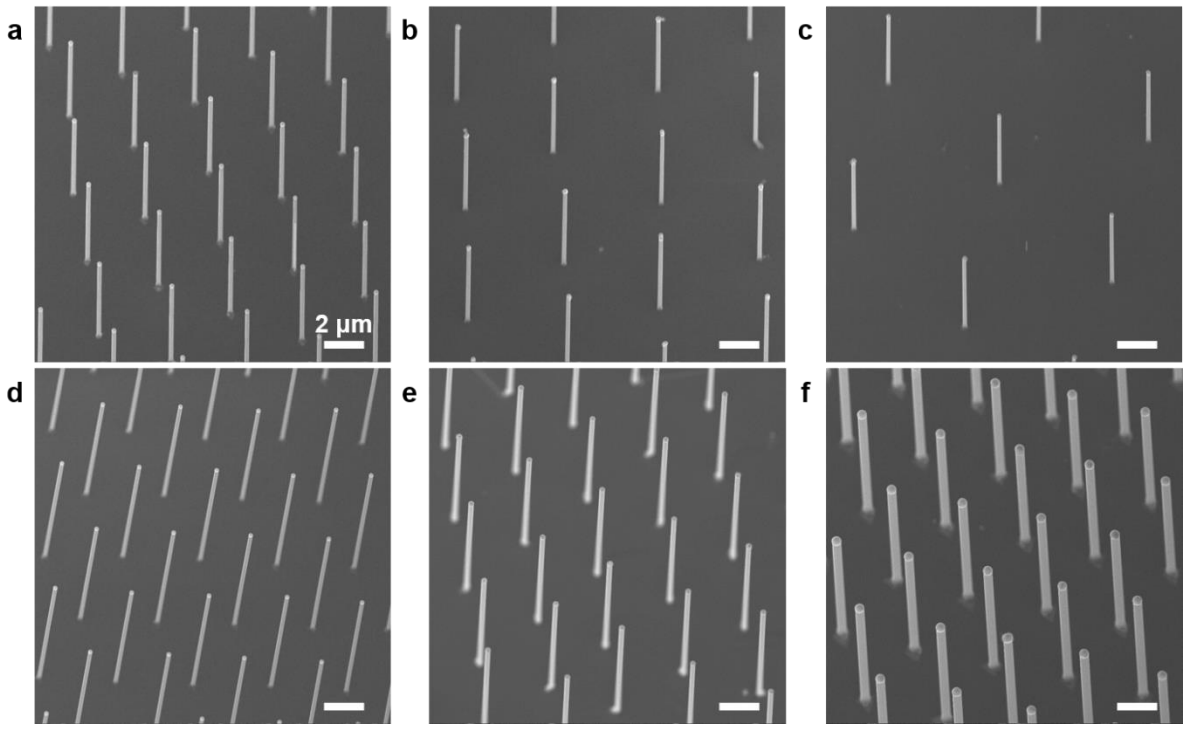

Figure S6. Controlled growth of *v*-SiNW arrays. Tilt-view (20°) SEM images of *v*-SiNW arrays after VLS growth with pitches of (a) 4, (b) 6, and (c) 8 μm, and with diameters of (d) 217, (e) 302, and (f) 443 nm, respectively. All *v*-SiNW arrays have (a–c) diameter D = 200 nm and length L = 10 μm, and (d–f) pitch P = 4 μm and length L = 12 μm. All scale bars are 2 μm.

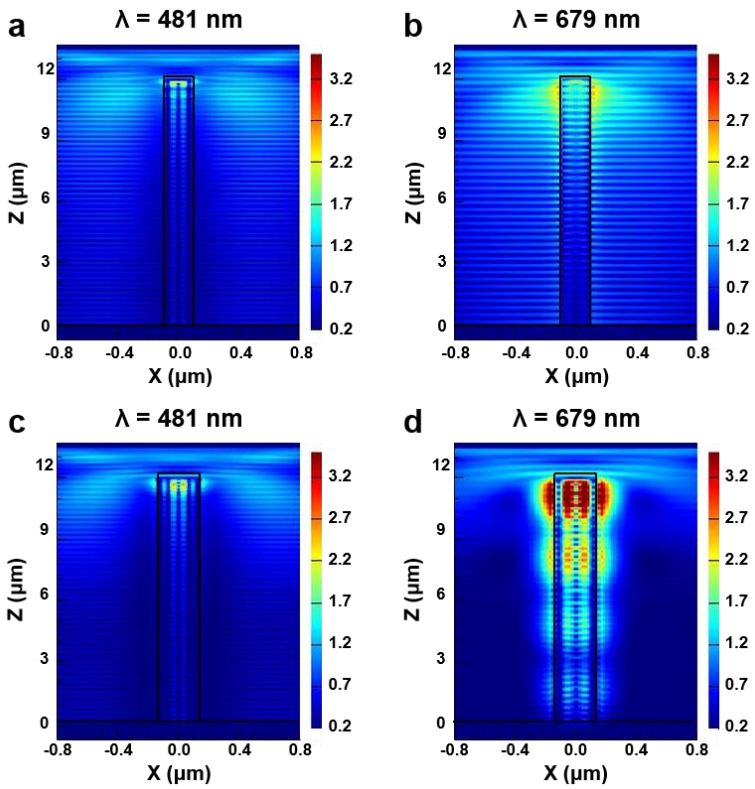

Figure S7. Diameter-dependent electric field distribution of a *v*-SiNW. Two-dimensional electric field distribution of SiNWs with diameter of (a, b) 200 and (c, d) 300 nm for wavelength for (a, c) 481 and (b, d) 679 nm, respectively, obtained by FDTD simulations.

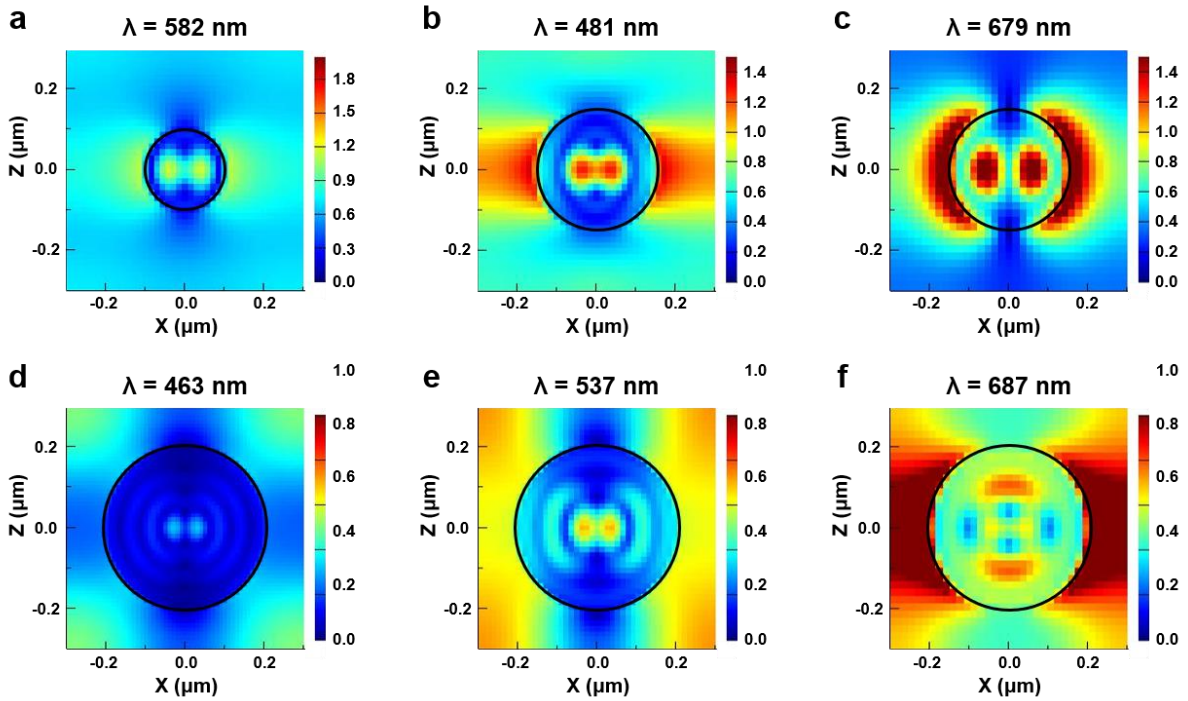

Figure S8. Geometry-dependent wavelength selective waveguiding with horizontal cross-sectional view. (a-f) Two-dimensional electric field distributions of SiNWs with different diameters of (a) 200 nm, (b,c) 300 nm, and (d–f) 400 nm for wavelength of (a) 582, (b) 481, (c) 679, (d) 463, (e) 537, and (f) 687 nm, respectively, obtained by FDTD simulations. Black circles outline the edges of the SiNW.

Section S3. Synthesis of tapered SiNWs.

The tapered *v*-SiNW arrays can be synthesized by changing experimental parameters, such as the growth temperature and H_2/Ar ratio. In this experiment, $SiCl_4$ is carried by H_2 gas and Ar is fed directly into the reactor. The 20° tilt-view SEM images of *v*-SiNW arrays synthesized with different H_2/Ar ratios of (a) 0.5 at 850 °C, (b) 0.2, and (c) 0.1 at 920 °C with fixed $SiCl_4$ molar fraction are shown (Figure 4a–c). The tapered SiNWs can be obtained by increasing the growth temperature and flow rate of Ar because the area of the nucleus for SiNW growth increases with increase in the growth temperature. A large amount of vapor-phase Si precursor ($SiCl_4$) precursors is introduced from the reservoir containing $SiCl_4$ solution (in accordance with Bernoulli's theorem) with increasing flow rate of Ar (Figure S1 for details of the reactor). Since the amount of Si precursor increases, the SiNWs tapered because of the epitaxial Si deposition on the sidewalls leading to VS growth.

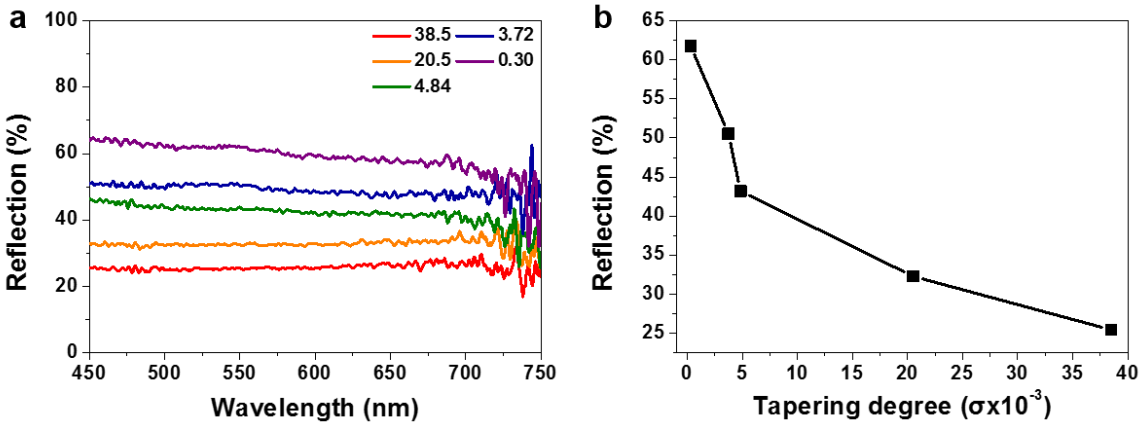

Figure S9. Tapering degree-dependent antireflection properties of *v*-SiNW arrays. (a) Measured reflection spectra of *v*-SiNW arrays with different tapering degrees ($\sigma \times 10^{-3}$). (b) Measured spectral reflection positions as a function of tapering degree ($\sigma \times 10^{-3}$).

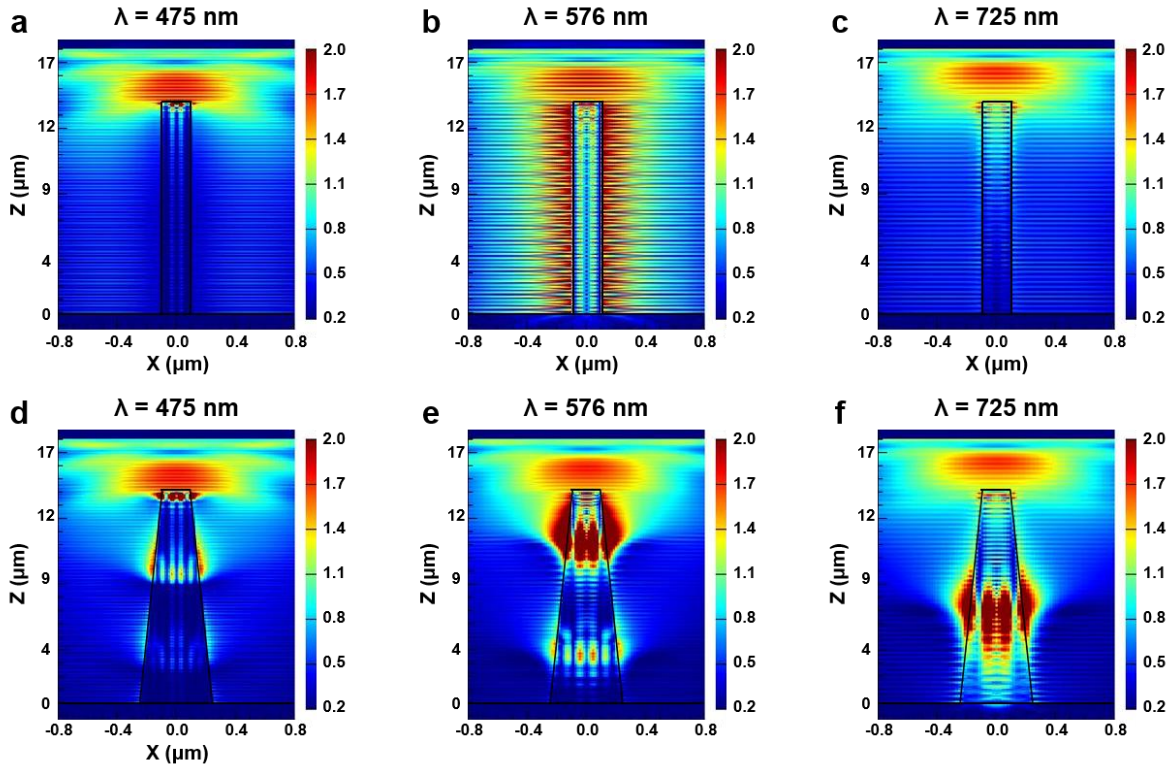

Figure S10. Shape-dependent electric field distribution of a *v*-SiNW. Two-dimensional electric field distributions of (a–c) straight (D_T = 200 nm, D_B = 200 nm) and (d–f) slightly tapered (D_T = 200 nm, D_B = 500 nm) SiNWs showing diameter selectivity for wavelengths of (a,d) 475, (b,e) 576, and (c,f) 725 nm, respectively, obtained by FDTD simulations. In addition, there is only one absorption resonance wavelength (λ = 576 nm) for the straight SiNW, which corresponds to results shown in Figure 4d. On the other hand, the slightly tapered SiNW shows three different electric field focused areas at λ = 475, 576, and 725 nm for reasons similar to observations recorded for tapered SiNW (Figure 4i–k).